INVITED PAPER

The Hallmarks of Mathematical Oncology

This article reviews classes of mathematical models used to understand and treat cancer, with the perspective of upcoming validated and clinically applicable cancer models.

By Joshua Adam Bull and Helen Mary Byrne

ABSTRACT | Over the past 25 years, there has been an unparalleled increase in understanding of cancer biology. This transformation is exemplified by Hanahan and Weinberg's decision in 2011 to expand their original Hallmarks of Cancer from six traits to ten! At the same time, mathematical modeling has emerged as a natural tool for unraveling the complex processes that contribute to the initiation and progression of cancer, for testing hypotheses about experimental and clinical observations and assisting with the development of new approaches for improving its treatment. This article starts by reviewing some of the earliest models of tumor growth and tumor responses to radiotherapy. Following Hanahan and Weinberg's lead, attention then focuses on how closer collaboration with cancer scientists and access to experimental data are stimulating the development of new and increasingly detailed models that account, for example, for tumor–immune interactions and immunotherapy. The article concludes by discussing the ways in which mathematical modeling is being integrated with experimental and clinical studies, and outlining how this could improve disease diagnosis and the delivery of effective personalized treatments to cancer patients. As such, this article serves as an introduction to mathematical modeling of cancer and its treatments, suitable for researchers seeking to enter the field.

KEYWORDS | Biology; mathematical model; medicine; Oncology; systems biology.

I. INTRODUCTION

A. Hallmarks of Cancer

Cancer is a generic term for a group of diseases that can affect any part of the body. While tremendous progress has been made in increasing our understanding of how tumors grow and improving their response to treatment, the worldwide burden of cancer incidence and mortality continues to grow, with approximately 19.3 million new cases and 10.0 million cancer-related deaths in 2020 [1]. These statistics highlight the complex and diverse nature of cancer and the continued need to increase understanding of how cancers develop and how treatments should be delivered to maximize the therapeutic benefit for individual patients.

Defining features of cancer include the rapid accumulation of abnormal cells that invade adjoining parts of the body and spread, or metastasize, to other organs. In 2000, Hanahan and Weinberg [2] introduced a conceptual framework for understanding the diversity of cancer in terms of six defining features or hallmarks: sustaining proliferative signaling, evading growth suppressors, activating invasion and metastasis, enabling replicative immortality, inducing angiogenesis (i.e., the growth of new blood vessels from existing ones), and resisting cell death. Hanahan and Weinberg [2] proposed that the transformation of normal cells to cancer cells requires the successive accumulation of multiple hallmarks, and cancer's diversity reflects the multiple ways in which they may be acquired. In 2011, increased understanding of cancer biology led Hanahan and Weinberg [2] to introduce four new hallmarks: avoiding immune destruction, deregulating cellular energetics, tumor-promoting inflammation, and genomic instability and mutation (see Fig. 1 and [3]).

B. Hallmarks of Mathematical Oncology

The Hallmarks of Cancer provide a conceptual framework for understanding different facets of cancer biology and why it is such a diverse disease. However, with verbal reasoning alone, it is difficult to understand how, for a particular individual, the order in which the hallmarks occur impacts their tumor's growth dynamics and/or response to treatment. The main aim of this article is to illustrate how mathematical modeling can provide a complementary

Manuscript received August 23, 2021; revised December 7, 2021; accepted December 15, 2021. Date of publication February 1, 2022; date of current version May 19, 2022. This work was supported by Cancer Research UK (CRUK) through the CRUK Oxford Centre under Grant C5255/A18085. *(Corresponding author: Joshua Adam Bull.)*

The authors are with the Mathematical Institute, University of Oxford, Oxford OX2 6GG, U.K. (e-mail: joshua.bull@maths.ox.ac.uk; helen.byrne@maths.ox.ac.uk).

Digital Object Identifier 10.1109/JPROC.2021.3136715

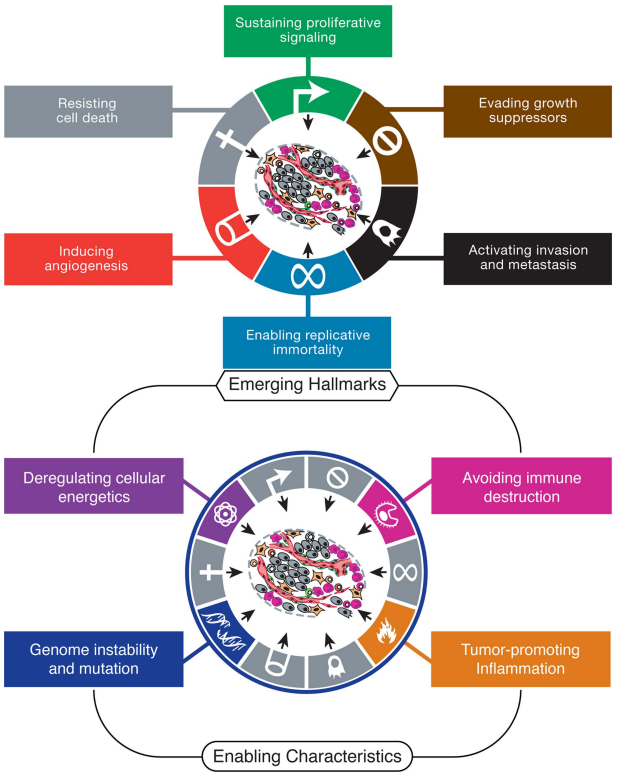

Fig. 1. ***Hallmarks of Cancer, as described by Hanahan and Weinberg [3]. Figure reproduced from [3, Figs. 1 and 3].***

framework for addressing these and related questions. Fig. 2 shows the Hallmarks of Mathematical Oncology, a conceptual framework that we introduce to characterize mathematical models. Each hallmark represents a modeling decision that determines the level of biological detail considered, the complexity of generating model solutions, and the types of data that the model can reproduce.

We identify six key mathematical hallmarks or decisions: single versus hybrid frameworks, homogeneity versus heterogeneity, spatially averaged versus spatially resolved, single-scale versus multi-scale, deterministic versus stochastic, and continuum versus discrete. Different mathematical models of cancer combine these hallmarks in different ways, leading to models that may include more biological complexity but are more challenging to analyze and/or parameterize. The glyphs in Fig. 2 (bottom) use the mathematical hallmarks to illustrate the increasing complexity of different modeling approaches. In this article, we explain how these frameworks can be used to model the same biological phenomena (responses to treatment with cancer radiotherapy) in increasing levels of detail.

By studying a series of increasingly detailed models, we aim also to demonstrate the additional insight that increased biological complexity and realism enable, and the need to balance these benefits against the costs. For example, with limited experimental data, it may not be possible to validate a complex model or to estimate the values of its parameters.

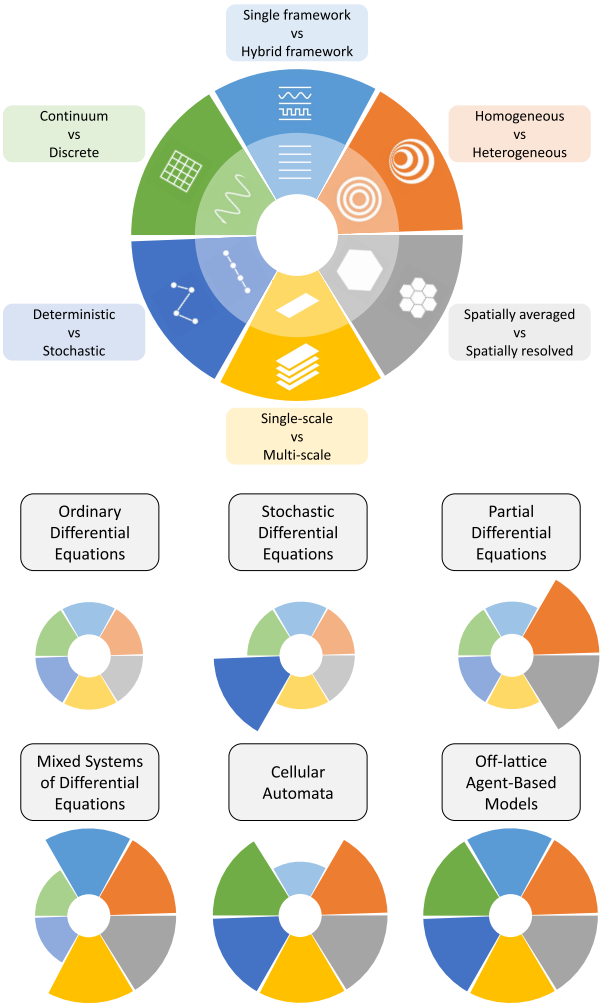

Fig. 2. ***Top: Hallmarks of Mathematical Oncology, a schematic illustrating the approaches used to develop mathematical models. Bottom: series of glyphs showing how different modeling frameworks may incorporate different mathematical hallmarks. Approaches that require additional complexity in mathematical hallmarks may resolve more detailed biological processes than simpler frameworks.***

The literature on mathematical oncology is now so large that, in limited space, we must be selective. We have chosen to focus on three modeling approaches that have been used to investigate solid tumor growth and tumor responses to radiotherapy (the following excellent texts provide further information about these and alternative modeling approaches: [4]–[6]). At the same time, we explain how more detailed modeling frameworks allow more detailed consideration of the factors limiting the efficacy of radiotherapy to be investigated, and assessment of strategies designed to compensate for these limitations.

The remainder of this article is organized as follows. In Section II, we provide a brief introduction to cancer biology and radiotherapy, and outline the process by which mathematical models are developed, tested, and refined. In Section III, we showcase simple models of solid tumor

growth, formulated using ordinary differential equations (ODEs), and explain how they can be adapted to predict radiotherapy responses. In Section IV, we introduce spatially resolved models, formulated using partial differential equations (PDEs), which can be used to investigate how spatial variation in cell density and nutrient levels impact the growth and composition of solid tumors. In Section V, we focus on agent-based models (ABMs) that can be used to investigate how the behavior of individual cells influences the dynamics at the tissue or macroscale. For each modeling approach, we also explain how the models can be extended to include more biological realism and, in particular, account for specific Hallmarks of Cancer. In Section VI, we outline the ways in which the different models are being integrated with experimental and clinical data. This article ends in Section VII with some general conclusions and future perspectives.

II. BIOLOGICAL AND MATHEMATICAL BACKGROUND

A. Biological Background

The multistage process by which normal cells transform into cancer cells, as embodied by the Hallmarks of Cancer, is associated with the progressive loss of function of a range of regulatory genes [2], [3]. These include repair genes that correct for mutations and DNA damage before cell division and tumor suppressor genes that signal for cell-cycle arrest or programmed cell death (apoptosis) if substantial genetic damage is detected. Uncontrolled cell division leads to the growth of (small) avascular tumors, which must recruit a new blood supply, via angiogenesis, to sustain their growth.

During avascular growth, nutrients are consumed by live, proliferating cells as they diffuse from the tumor periphery to its center. Therefore, as an avascular tumor grows, nutrient levels at its center decline until it reaches a critical size at which there is insufficient nutrient to sustain viable cells, a central core of dead (necrotic) cellular material forms, and its size increases as the tumor continues to grow. Thus, a well-developed, avascular tumor comprises an outer rim of nutrient-rich, proliferating cells, a central core of nutrient-starved, necrotic debris, and an intermediate layer of oxygen-poor (or hypoxic) cells that are quiescent (i.e., viable but nonproliferating). Since diffusion controls nutrient delivery to, and the removal of waste products from, avascular tumors [7], the diameter to which they may grow is limited to several millimeters, and they are relatively harmless. By contrast, vascular tumors are life-threatening for two main reasons. First, being connected to the host's blood supply, they have access to an almost limitless supply of nutrients. Their consequent rapid growth may impair the function of neighboring vital organs. Second, tumor fragments that break away from the primary tumor and enter blood vessels may be transported to other parts of the body where they establish secondary tumors (metastases) that further jeopardize the host. The switch from avascular to vascular growth is achieved by activating angiogenesis, a hallmark of cancer [8].

During angiogenesis, the tumor cells secrete multiple diffusible factors (e.g., vascular endothelial growth factor (VEGF) and tumor necrosis factor-β), known collectively as angiogenic factors, which stimulate endothelial cells from nearby blood vessels to proliferate and migrate toward the tumor, forming new vessels that supply it with the nutrients required for continued growth. Invasion of healthy tissue is another hallmark of cancer: contact with the healthy tissue stimulates the tumor cells to produce matrix-degrading enzymes (e.g., matrix metalloproteases) that create spaces into which the tumor cells can migrate [9]. At a cellular level, the sequence of events needed to establish a well-developed, vascularized tumor may be associated with mutations in a variety of genes. For example, it has been estimated that up to 50% of tumors harbor mutations in the tumor suppressor gene p53, and these mutations have been linked with angiogenesis and cell immortality, two Hallmarks of Cancer [10].

The above discussion underscores the complex and multiscale nature of solid tumor growth, with multiple biophysical processes interacting across a wide range of spatial and temporal scales. At the subcellular scale, individual cells produce proteins that regulate their behavior; at the cellular scale, normal and cancerous cells compete for space and nutrients, while behaviors at the macroscale include vascular remodeling, blood flow, and nutrient transport. Now, in response to environmental stresses, such as hypoxia, tumor cells may alter their subcellular behavior by slowing (or halting) the rate at which they progress through the cell cycle and/or altering the rate at which they produce angiogenic factors, such as VEGF. When released by the cell, the angiogenic factors diffuse through the tissue until they reach neighboring vessels where they stimulate the formation of new blood vessels and, thereby, increase the supply of nutrients to the tumor. In this way, phenomena at the subcellular and macroscale may interact. We will explore these ideas further in Section V, where we introduce multiscale models of tumor growth.

B. Radiotherapy

During radiotherapy, beams of ionizing particles are directed at cancer cells to kill them or slow their growth by inflicting single- and double-strand breaks on their nuclear DNA. A 1-Gy (1 Gy = 1 Gray = 1 Joule/kg) dose of gamma radiation causes approximately 1000 single-strand breaks and 20–25 double-strand breaks [11]. Cell survival following radiation depends on fully functioning DNA damage repair mechanisms, with cell death triggered only when double-strand breaks are not properly repaired. Typically, only 1%–2% of double-strand breaks are lethal, and the number of cells that survive exposure to radiotherapy is highly dependent on the dose rate [12]. Radiotherapy is most effective when it elicits favorable,

differential responses in the host and cancer cells, such as when the host cells have lower proliferation rates and better repair mechanisms than tumor cells.

Radiotherapy may be administered prior to surgery to shrink a tumor, during surgery to minimize damage to surrounding healthy tissue [13], and postsurgery to prevent the regrowth of any residual tumor cells. It is often combined with chemotherapy [14] and, increasingly, with treatments such as hyperthermia [15], virotherapy [16], and immunotherapy [17]. Typical radiotherapy protocols last for six to eight weeks, with treatment administered five days per week, with rest periods at weekends.

When directing radiotherapy at cancer cells, it is important to limit the damage to adjacent healthy tissue. Typically, treatment aims to maximize the cancer cell kill while ensuring that the damage sustained by neighboring healthy cells is within tolerable levels. In practice, additional factors also limit the efficacy of radiotherapy. For example, tumors may fail to respond to radiotherapy due to intrinsic or acquired (i.e., treatment-induced) resistance, with cancer stem cells viewed as one source of such resistance. Hypoxia, arising from the abnormal and poorly functioning tumor vasculature, is also a barrier to the efficacy of radiotherapy, with hypoxic cells estimated to be up to three times more radio-resistant than well-oxygenated cells. Novel strategies being designed to boost tumor oxygen levels and, thereby, enhance tumor radiosensitivity include hyperbaric oxygen and metabolic inhibitors [18], [19].

The linear-quadratic (LQ) model is widely used to calculate the fraction SF of cells that survive exposure to n fractions of radiotherapy with dose d, delivered over the time period $0 < t < t_{\text{end}}$

$$\text{SF} = \frac{V\left(t = t_{\text{end}}\right)}{V\left(t = 0\right)} \equiv \exp\left(-n\left(\alpha d + \beta d^2\right)\right) \tag{1}$$

where the positive constants α and β are tumor-specific radiosensitivity parameters, and $V(t = 0)$ and $V(t = t_{\text{end}})$ denote the initial and final tumor volumes [20].

When the survival fraction is plotted on a log scale, we observe a quadratic dose–response. The response is dominated by the linear (α) term at low doses and by the quadratic (β) term at higher doses, with the ratio α/β representing the dose at which the linear and quadratic terms are equal. Thus, the cell kill for cells with high α/β ratios remains relatively constant with increasing dose and increases markedly for those with low α/β ratios. We may interpret the linear term as describing cell death from a "single hit" (i.e., lethal damage caused by a single radiation track), while the quadratic term describes cell death due to "multiple hits." In practice, the cell death induced by exposure to radiotherapy occurs over a finite time period: the LQ model accounts for these dynamics implicitly, quantifying the total cell kill in terms of the radiotherapy dose d and the values of the parameters α and β, and not explicitly resolving the temporal dynamics.

While some authors have derived the LQ model from a mechanistic perspective (e.g., relating the dose to the numbers of single- and double-stranded DNA breaks and then relating the numbers of such DNA breaks to the cell kill) [21], it was originally developed to provide a phenomenological description of experimental observations of the dose–response relationship. Although the LQ model is widely used to predict tumor responses to radiotherapy, it has several shortcomings. For example, in its simplest form, the LQ model does not account explicitly for the five R's of radiotherapy: Repair, Repopulation, Redistribution of cells around the cell cycle, Reoxygenation, and radio Resistance [22]. While the LQ model has been extended to account for these effects [23], [24], the relationships between dose and the five R's are complex and often neglected—indeed, some argue that results generated from more complex dose–response models yield results that are equivalent to those of the original LQ model [21]. A further weakness of the LQ model is that it lacks explicit time-dependence, focusing only on the total cell kill achieved by a dose d of radiotherapy. Alternative models have been proposed, which explicitly account for time-dependent responses to treatment (e.g., [25]–[27]).

The mathematical models introduced in this article will illustrate how the five R's of radiotherapy can be modeled through appropriate choices of the Hallmarks of Mathematical Oncology.

C. Modeling Approaches

Statistical techniques, applied to experimental data, can reveal correlations between observable phenomena. Establishing why such correlations arise requires the statement of hypotheses that propose which physical processes are involved and how they interact. The biological experiments needed to verify these hypotheses can be time-consuming and challenging to undertake. In such circumstances, mathematical models can be used to test the consistency of the hypotheses. In particular, if a mathematical model is unable to reproduce the observed phenomena, then the hypotheses should be revised before continuing. Mathematical models can also improve experimental design by highlighting which data should be collected to test a particular theory.

Fig. 3 serves as a guide to the stages involved in developing and refining mathematical models. It also shows that mathematical modeling is an iterative process, whose success relies on continued multidisciplinary collaboration between experimentalists and theoreticians.

While Fig. 3 provides a roadmap for developing, testing, and exploiting mathematical models, it sidesteps a key aspect of model building: deciding what mathematical approach or framework should be used to formulate the mathematical model. Many alternative approaches can be used, as illustrated by the mathematical hallmarks outlined

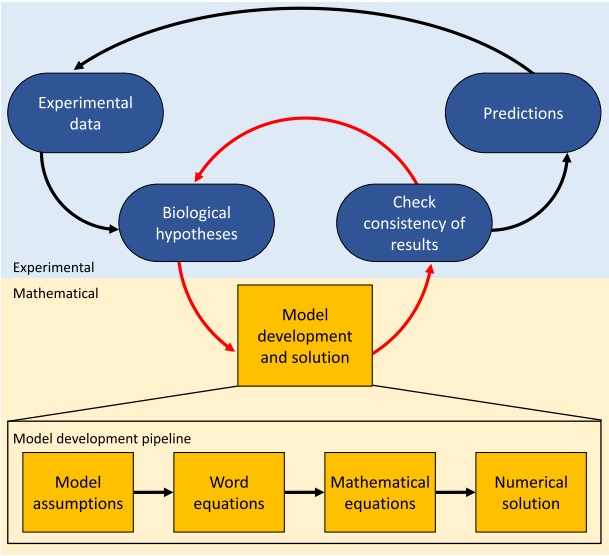

Fig. 3. *Schematic highlighting the iterative and multidisciplinary nature of mathematical modeling. Experimental data guide the generation of biological hypotheses that can be formalized in mathematical models. Model validation involves establishing consistency between model solutions and the experimental data. If this is not obtained, then the hypotheses and models must be revised until qualitative and quantitative agreements are reached. Parameter values can be estimated by fitting the model to the data, and the model is then used to generate experimentally testable predictions.*

in Fig. 2; the models may be deterministic, comprising systems of time-dependent ordinary and/or PDEs, or they may be stochastic, accounting for random effects; they may be based on physical principles (e.g., Newton's laws of mechanics) or phenomenological in nature; they may focus on processes that happen on a specific spatial and/or temporal scale (e.g., subcellular signaling pathways); or they may be multiscale, coupling processes acting at the subcellular, cellular, and tissue scales. With such an array of choices, it can be difficult to know how to proceed. In practice, decision-making should be guided by the questions that the modeling is designed to address and the quality and quantity of data available for model testing and validation.

In the remainder of this article, we aim to clarify these concepts by introducing a series of modeling approaches, outlining the assumptions on which they are based, highlighting the insight that they can provide, their possible extensions, and their limitations. We start by focusing on arguably the simplest class of mathematical models: those that can be formulated using ODEs.

III. ORDINARY DIFFERENTIAL EQUATION MODELS

In this section, we introduce several idealized models of solid tumor growth. Spatial effects are neglected, and the models are formulated as systems of time-dependent ODEs. This corresponds to the simplest selection of mathematical hallmarks in Fig. 2, with the tumor viewed as a spatially uniform and homogeneous cell population. We explain how models of this type may be used to determine how a tumor's volume changes over time and integrated with models of cell kill due to radiotherapy in order to predict its impact and compare different protocols for its delivery.

A. Tumor Growth Models

Arguably, the simplest model that describes how the volume of a solid tumor V evolves over time is the exponential growth law that states

$$\frac{dV}{dt} = \lambda V, \quad \text{with } V(t=0) = V_0 \tag{2}$$

with solution

$$V(t) = V_0 e^{\lambda t}.$$

In (2), $\lambda > 0$ and V_0 represent the net growth rate of the tumor and its initial volume, respectively. In this model, there are no growth constraints: all nutrients and growth factors are assumed to be in abundance. As a result, the model predicts the unbounded growth of the tumor.

While providing an accurate description of the early stages of a tumor's development, the exponential growth law fails to describe the reduced growth rates and eventual growth saturation observed when avascular tumors are cultured *in vitro* or when vascular tumors develop *in vivo*. In practice, the tumor's growth rate slows because, as it increases in size, competition for nutrients and other vital resources, such as space, can no longer be neglected. A simple modification of (2) that accounts for competition for resources (without specifying what those resources are) is the logistic growth law

$$\frac{dV}{dt} = \lambda V\left(1 - \frac{V}{K}\right), \quad \text{with } V(t=0) = V_0 > 0 \tag{3}$$

with solution

$$V(t) = \frac{KV_0}{V_0 + (K - V_0)e^{-\lambda t}}$$

where $K > 0$ represents the population's carrying capacity. Thus, at large times, the tumor volume $V(t)$ approaches the carrying capacity, K.

While (3) predicts exponential growth of small tumors and growth saturation when the tumor reaches its carrying capacity ($V = K$), we note that it has only two parameters: λ and K. These parameters determine the tumor volume at which growth saturates (K) and its growth rate. In practice, when fitting to experimental data, a model that offers greater flexibility in the growth dynamics may be desirable. For example, the generalized logistic model extends the logistic model by introducing an additional

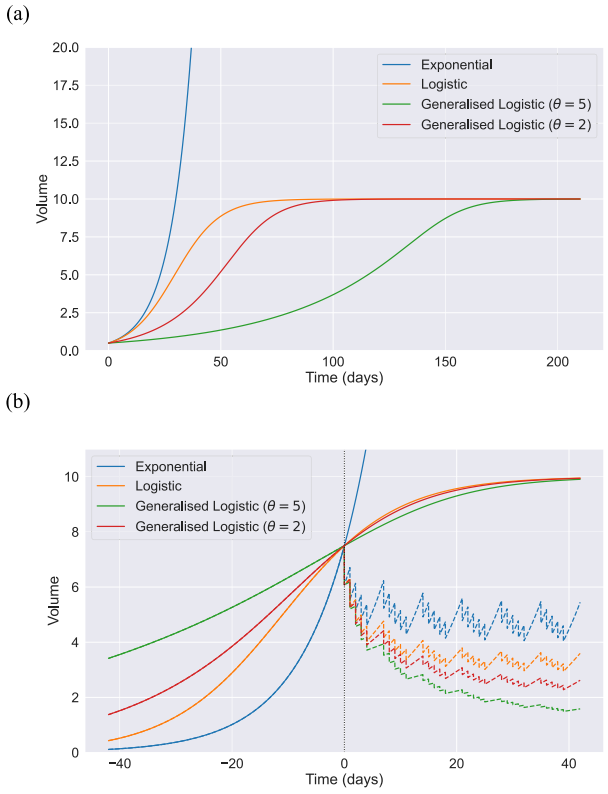

Fig. 4. *Series of curves showing how the choice of growth law influences (a) a tumor's growth dynamics and (b) its response to radiotherapy. Key: exponential growth law (blue, $\lambda = 0.1$); logistic growth law (orange, $\lambda = 0.1, K = 10$); and generalized logistic growth law (green, $\lambda = 0.1, K = 10, \theta = 5$; red, $\lambda = 0.1, K = 10, \theta = 2$). (b) Solid lines show untreated tumor growth, and dashed lines show the effect of treating the tumor with daily doses of 2 Gy of radiotherapy on weekdays beginning when each model reaches $v = 7.5$ at $t = 0$ (cell kill based on the linear quadratic model, with $\alpha = 0.01$ and $\beta = 0.001$).*

parameter, $\theta > 0$, which allows greater flexibility over the growth dynamics. This model is given by

$$\frac{dV}{dt} = \frac{\lambda}{\theta} V \left[1 - \left(\frac{V}{K}\right)^{\theta}\right], \quad \text{with } V(t=0) = V_0 \tag{4}$$

with solution

$$V(t) = K\left(\frac{V_0^{\theta}}{V_0^{\theta} + \left(K^{\theta} - V_0^{\theta}\right) e^{-\lambda t}}\right)^{1/\theta}.$$

We remark that (4) reduces to (3) when $\theta = 1$.

In Fig. 4(a), we compare the three models described above, presenting plots of the growth dynamics defined by (2)–(4) for fixed values of λ, K, two values of θ, and the same value of V_0, the initial tumor volume. Many other growth laws have been used to describe solid tumor growth [28]. Increasing the number of model parameters results in more flexible growth dynamics and, therefore, a better fit to clinical or experimental data. However, using more complex models can result in overfitting and, hence, reduce the biological insight available from a model. To counter this, model selection methods, such as Akaike's information criteria (AIC) and Bayesian information criteria (BIC), have been developed in order to balance the fit of a model against model complexity (see [29]).

A common weakness of the ODE models introduced in this section is the difficulty of relating the system parameters [e.g., λ, K, and θ in (4)] to the behavior of individual cells. We return to this matter in Sections IV and V where we discuss spatially structured models of tumor growth. First, we explain how the ODE models can be used to gain preliminary insight into how tumors respond to radiotherapy.

B. Tumor Growth and Radiotherapy

For simplicity, we will consider a tumor which undergoes exponential growth in the absence of treatment [see (2)]. We suppose that n fractions of radiotherapy, with dose d, are administered at times t_i $(i = 1, 2, 3, \ldots, n)$, the resulting cell kill is instantaneous, and the fraction SF of cells that survive each dose of radiotherapy can be described by the LQ model [see (1)]. Under these assumptions, it is possible to show that the following ODE describes exponential growth between fractions and cell kill due to radiotherapy [30]:

$$\frac{dV}{dt} = \lambda V - \sum_{i=1}^{n} \left(\alpha d + \beta d^2\right) V \delta\left(t - t_i\right) \tag{5}$$

where $V(t=0) = V_0 > 0$ and $\delta(t)$ denotes the Dirac delta function [for an arbitrary smooth function, $f(t)$, the delta function is defined so that $\int_{-\infty}^{+\infty} f(t)\delta(t - t_i)dt = f(t_i)$]. Solving (5) subject to $V(t=0) = V_0 > 0$, we obtain

$$V(t) = V\left(t_i^+\right) e^{\lambda(t - t_i)}, \quad \text{for } t_i^+ \le t \le t_{i+1}^- \tag{6}$$

$$\text{where } V\left(t_i^+\right) = V\left(t_i^-\right) e^{-\left(\alpha d + \beta d^2\right)} \tag{7}$$

and $V(t_i^-)$ and $V(t_i^+)$ denote the tumor volumes immediately before and after radiotherapy, and $V(t_i^+)/V(t_i^-) \equiv \text{SF}$ [see (1)]. Combining (6) and (7), we deduce further that

$$\text{SF} = \frac{V\left(t_n^+\right)}{V(0)} \equiv \underbrace{e^{\lambda t_n}}_{\substack{\text{contribution} \\ \text{due to growth}}} \cdot \underbrace{e^{-n\left(\alpha d + \beta d^2\right)}}_{\substack{\text{contribution due} \\ \text{to radiotherapy}}}. \tag{8}$$

In particular, if growth is neglected (i.e., $\lambda = 0$), then (8) reduces to (1). Thus, (8) makes explicit how, by coupling the LQ model with an ODE model for (exponential) tumor growth, it is possible to extend the LQ model to account for the combined effects of tumor growth and cell kill due to radiotherapy.

By suitable rearrangement of (3) and (4), it is possible to combine cell kill due to radiotherapy with the logistic and generalized logistic growth laws in a similar manner. The corresponding ODEs are

$$\frac{dV}{dt} = \lambda V \left[1 - \left(\frac{V}{K}\right)^{\theta}\right] - \sum_{i=1}^{n} \left(\alpha d + \beta d^2\right) V \delta\left(t - t_i\right) \quad (9)$$

with $V(t=0) = V_0 > 0$ and $\theta = 1$ for the logistic growth law. The simulation results presented in Fig. 4(b) show how radiotherapy affects tumor growth, for the three models introduced in Section III-A. Each model exhibits the same, "sawtooth" dynamics, with tumor regrowth between radiotherapy doses and rapid (instantaneous) reductions in tumor volume when radiotherapy is administered. While the qualitative behavior for each model is similar, for this set of parameter values, the long time dynamics differ: the exponential growth model predicts the smallest reduction in tumor volume and the two generalized logistic models the largest reduction. The variability in the model predictions highlights the importance of being able accurately to model a tumor's growth dynamics in order to accurately predict its response to radiotherapy.

The simulation results presented in Fig. 4 assume that the cell survival fraction following radiotherapy is governed by the LQ model. While the LQ model is widely used in the clinic, we emphasize that it is phenomenological. Other authors have proposed alternative models of radiotherapy. Zahid *et al.* [31] propose a novel approach in which radiotherapy doses instantaneously reduce the carrying capacity of the tumor in the logistic model, rather than directly affecting the tumor volume. In another example, Prokopiou *et al.* [32] proposed the following model for tumor response to radiotherapy:

$$\frac{dV}{dt} = \lambda V \left(1 - \frac{V}{K}\right) - \sum_{i=1}^{n} \gamma V \left(1 - \frac{V}{K}\right) \delta\left(t - t_i\right) \quad (10)$$

where γ is a parameter describing the response to radiotherapy. Equation (10) assumes that the tumor undergoes logistic growth, and the instantaneous cell kill due to radiotherapy is proportional to the logistic growth rate. A key assumption underpinning this model is that, when a tumor reaches its carrying capacity, the proportion of cells that are actively proliferating approaches zero. Since radiotherapy is more effective at killing proliferating cells, the cell kill also reduces as the tumor approaches its carrying capacity. These assumptions contrast with those for the LQ model, which assumes that the cell kill is proportional to the tumor volume when radiotherapy is administered (and does not reduce as the tumor approaches its carrying capacity). Comparison of (5) and (10) illustrates the importance of understanding the assumptions on which a mathematical model is based. In particular, a tumor that approaches its carrying capacity because its (positive) rates of cell proliferation and cell death balance will remain sensitive to radiotherapy as it approaches its carrying capacity. By contrast, a tumor in which the proportion of proliferating cells diminishes as it approaches its carrying capacity will become less radio-sensitive as it approaches its carrying capacity.

C. Model Extensions

A common, simplifying assumption of the above ODE models is tumor homogeneity, both with regard to cell phenotypes and spatial variation across the tumor. In practice, however, tumors exhibit spatial and cellular heterogeneity. In Sections IV and V, we introduce models that account for spatial heterogeneity. First, we outline how ODE models can be adapted to account for tumor heterogeneity and to investigate the impact of several Hallmarks of Cancer (e.g., inducing angiogenesis, resisting cell death, tumor-promoting inflammation, and avoiding immune destruction: see Fig. 1) on tumor growth and response to radiotherapy.

While it is possible to develop ODE models that account for vasculature, immune cells, and different subpopulations of healthy and cancerous cells, mathematical models typically focus on a limited number of species. For example, in [33], the classical Lotka–Volterra model is used to study the dynamics of cocultured populations of radiosensitive and radio-resistant tumor cells and to investigate whether exposure to radiotherapy alters the way in which they interact. In the absence of radiotherapy, the governing equations can be written as

$$\frac{dV_S}{dt} = \lambda_S V_S \left(1 - \frac{V_S}{K_S} - \gamma_R \frac{V_R}{K_S}\right) \quad (11)$$

$$\frac{dV_R}{dt} = \lambda_R V_R \left(1 - \frac{V_R}{K_R} - \gamma_S \frac{V_S}{K_R}\right) \quad (12)$$

where $V_S(t)$ and $V_R(t)$ represent the volumes of the control and resistant populations, λ_S and λ_R their growth rates, and K_S and K_R their carrying capacities, so that, if $V_R = 0$, then the radiosensitive cells undergo logistic growth (and vice versa). The parameters γ_S and γ_R describe the effect that the radiosensitive cells have on the resistant cells (and vice versa): if $\gamma_S > 0$ and $\gamma_R > 0$, then the interactions are competitive, i.e., the presence of one cell type inhibits the growth of the other. If $\gamma_S < 0$ and $\gamma_R < 0$, then interactions are mutualistic since the presence of one cell type enhances the growth of the other. Finally, if γ_S and γ_R have opposite signs, then the interactions are antagonistic since interactions in one direction are beneficial and in the other are detrimental (e.g., if $\gamma_R < 0 < \gamma_S$, then the growth of sensitive cells is enhanced by resistant cells, while resistant cells are hindered by sensitive cells).

Similar ODE models have been proposed to describe the impact on tumor growth and radiotherapy responses of the vasculature [34], [35] and the immune system [36], [37], and also to explore the efficacy of treatments that combine radiotherapy with, for example,

chemotherapy [38], antiangiogenic therapy [35], and virotherapy [39].

The LQ model assumes that cell death following exposure to radiotherapy is instantaneous, and any dead material is eliminated from the tumor immediately. These assumptions give rise to the sawtooth dynamics depicted in Fig. 4. In practice, such dead material is removed (or phagocytosed) by immune cells over a finite time period, leading to behaviors which differ from the sawtooth dynamics. This can be addressed by including multiple model compartments that account for viable cells and lethally damaged cells [40]. For example, Lewin *et al.* [41] have developed an ODE model that distinguishes viable tumor volume [$V(t)$] and dead or necrotic material [$N(t)$] and accounts for degradation of dead material

$$\frac{dV}{dt} = \lambda V\left(1-\frac{V}{K}\right) - \eta V - \gamma\sum_{i=1}^{n} V\delta\left(t-t_i\right) \tag{13}$$

$$\frac{dN}{dt} = \eta V - \zeta N + \gamma\sum_{i=1}^{n} V\delta\left(t-t_i\right). \tag{14}$$

In addition to undergoing logistic growth, the viable tumor cells undergo necrosis at a constant rate η. The necrotic material undergoes exponential decay at a constant rate ζ. Fractionated radiotherapy, delivered at times t_i, causes instantaneous mass exchange between the viable and necrotic compartments. The dead material is unaffected by radiotherapy, and so, radiation-induced cell death is proportional to the viable tumor volume, V, with death rate γ, which contrasts with the corresponding terms using in (9) and (10) where the logistic term is assumed to encompass the population of cells sensitive to irradiation. Extensive model simulations reveal how this two-compartment model may better capture the full range of dynamics observed *in vivo* (see Section VI and Fig. 10 for more details).

When using ODE models to simulate tumor shrinkage during treatment with radiotherapy, we must be mindful of their limitations. In particular, as the tumor volume becomes very small (e.g., below the size of ten or fewer cells), stochastic effects become important, and the validity of using differential equations to describe the system dynamics breaks down. In such cases, stochastic models can be developed to describe the system dynamics and predict the probability of tumor elimination in response to treatment [25].

IV. PDE MODELS

Many cell functions depend on their microenvironment. For example, in well-oxygenated regions, tumor cells proliferate rapidly and are highly sensitive to radiotherapy. By contrast, in hypoxic regions, cells reduce, or halt, their cell cycle and are less sensitive to radiotherapy. ODE models are unable to account for the effects that environmental and cellular heterogeneities have on a tumor's spatial composition, its growth dynamics, and its response to treatment. In this section, we introduce two models that use PDEs to investigate the effects that spatial variation in the local microenvironment and the tumor cell density have on tumor growth. We term these models *the Greenspan model* [42] and the *proliferation-invasion model* [43].

A. Greenspan Model

Greenspan's model is one of the earliest models to account for spatial heterogeneity. It considers a radially symmetric tumor whose growth is regulated by a single, diffusible growth factor that is supplied externally (here taken to be oxygen). The distribution of the growth factor within the tumor regulates its local behavior, with volumetric growth where cell proliferation exceeds cell death (and vice versa). By integrating these contributions over the tumor volume, we arrive at the following equation that relates the time evolution of the tumor volume $V(t)$ to the oxygen concentration $c(r,t)$ within the tumor volume

$$\frac{dV}{dt} = \int_{\partial V} F\left(c\right) dV \tag{15}$$

where $F(c)$ describes the dependence on local oxygen levels of the net growth rate. Under the assumption of radial symmetry, $V(t) = \frac{4}{3}\pi R^3(t)$, where $R(t)$ denotes the position of the tumor boundary, and (15) reduces to give

$$\frac{dR}{dt} = \frac{1}{R^2}\int_0^{R(t)} F\left(c\right) r^2 dr \tag{16}$$

with $R(0) = R_0$ prescribed. The oxygen distribution is governed by a reaction–diffusion equation of the form

$$\frac{\partial c}{\partial t} = \frac{1}{r^2}\frac{\partial}{\partial r}\left(r^2\frac{\partial c}{\partial r}\right) - G\left(c\right) \tag{17}$$

with boundary and initial conditions of the form

$$c\left(R\left(t\right),t\right) = c_\infty, \quad \text{on } r = R\left(t\right) \tag{18}$$

$$\frac{\partial c}{\partial r} = 0, \quad \text{at } r = 0 \tag{19}$$

$$c\left(r,0\right) = c_0\left(r\right), \quad \text{for } 0 \le r \le R_0 \tag{20}$$

where $G(c)$ and c_∞ denote the oxygen consumption rate and the assumed constant oxygen concentration on the tumor boundary, and $c_0(r)$ is the oxygen distribution within the tumor at $t = 0$.

For simplicity (and without appropriate data to justify more complex functions), Greenspan and many others have used idealized functional forms for $F(c)$ and $G(c)$ of the form

$$F\left(c\right) = s_0 c H\left(c-c_H\right) - \mu_A - \mu_N H\left(c_N - c\right) \tag{21}$$

$$G\left(c\right) = \Gamma H\left(c-c_N\right) \tag{22}$$

where H is the Heaviside function ($H(x) = 1$ if $x > 0$, and $H(x) = 0$ otherwise), and c_H and c_N are oxygen thresholds below which cells become hypoxic ($c \leq c_H$) and necrotic ($c \leq c_N < c_H$). Thus, in well-oxygenated regions, where $c > c_H$, cells proliferate, at a rate proportional to their local oxygen concentration, with constant of proportionality s_0, undergo natural or apoptotic cell death at rate μ_A, and consume oxygen at a constant rate Γ. In low-oxygen regions (i.e., under hypoxia), where $c_N < c < c_H$, the cells do not proliferate or consume oxygen, but they undergo necrosis. In very-low-oxygen regions, where $c \leq c_N$, cells are unable to remain viable, and they undergo apoptotic and necrotic cell death, the latter at rate μ_N.

With cell proliferation and necrotic cell death occurring in distinct spatial regions, we can see how spatial heterogeneity can be incorporated within a PDE framework. Indeed, it is possible to identify the sizes of the proliferating, hypoxic, and necrotic regions by tracking the positions $r = R_H(t)$ and $r = R_N(t)$ at which the oxygen concentration attains the hypoxic and necrotic threshold values

$$R_H = 0, \quad \text{if } c > c_H \ \forall r \text{ and otherwise } c(R_H, t) = c_H \tag{23}$$

$$R_N = 0, \quad \text{if } c > c_N \ \forall r \text{ and otherwise } c(R_N, t) = c_N. \tag{24}$$

Following Lewin *et al.* [44], we can exploit the spatial heterogeneity of the Greenspan model to develop a description of tumor response to radiotherapy, which accounts for differential radiosensitivity in well-oxygenated and hypoxic regions: we replace (1) by a local survival fraction, $\mathrm{SF}(c)$, where

$$\mathrm{SF}(c) = \exp\left(-\left(\alpha \cdot \frac{d}{\mathrm{OER}(c)} + \beta \cdot \frac{d^2}{\mathrm{OER}^2(c)}\right)\right) \tag{25}$$

where the oxygen enhancement factor $\mathrm{OER}(c)$ is given by

$$\mathrm{OER}(c) = \begin{cases} 1, & \text{if } c > c_H \\ 3, & \text{if } c_N \leq c \leq c_H. \end{cases} \tag{26}$$

In Fig. 5, we present typical model solutions, showing tumor responses to a six-week fractionation protocol, where 2-Gy fractions are delivered daily Monday–Friday. As for the ODE models, the tumor radius undergoes sawtooth dynamics although we can now see how the tumor's spatial structure evolves. Fig. 6 shows how the oxygen concentration within the necrotic core fluctuates during the early stages of treatment. As successive doses of radiotherapy cause the tumor to shrink in size, oxygen levels at the center of the necrotic core increase, eventually rising above the necrotic and hypoxic thresholds. As treatment progresses, reoxygenation of previously hypoxic and necrotic regions combined with an increase in the proportion of the tumor occupied by proliferating cells leads to increased radiosensitivity and a corresponding reduction in the average survival fraction.

B. Proliferation-Invasion Model

While the Greenspan model incorporates heterogeneity due to spatial variations in oxygen levels, other types of heterogeneity are of interest when modeling tumor growth and radiotherapy. For example, when glioma cells, a common type of brain tumor, invade brain tissue, their motility and proliferation rates differ in gray and white matters. Swanson *et al.* [43], [45] proposed the following PDE model to describe how glioma cells move by random motion and proliferate in gray and white matter

$$\frac{\partial c}{\partial t} = \nabla \cdot (D(\mathbf{x}) \nabla c) + \rho c \tag{27}$$

where $c(\mathbf{x}, t)$ denotes the concentration of tumor cells at time t and position $\mathbf{x}$, and ρ is the net proliferation rate of the glioma cells. The diffusion coefficient $D(\mathbf{x})$ is piecewise constant, with $D(\mathbf{x}) = D_g, D_w$ in gray and white matter, and $D_w > D_g$ to account for the greater motility of glioma cells in white matter.

Equation (27) can be extended to account for additional effects. For example, the net proliferation term ρc can be replaced with a logistic growth model, giving

$$\frac{\partial c}{\partial t} = \nabla \cdot (D(\mathbf{x}) \nabla c) + \rho c \left(1 - \frac{c}{K}\right) \tag{28}$$

with carrying capacity K and constant growth rate ρ [46]. Rockne *et al.* [47] use this formulation of the PI model to account for death from radiotherapy using the LQ model

$$\frac{\partial c}{\partial t} = \nabla \cdot (D \nabla c) + \rho c \left(1 - \frac{c}{K}\right) - \left(1 - e^{-(\alpha d + \beta d^2)}\right) c \left(1 - \frac{c}{K}\right) \delta(t - t_i). \tag{29}$$

The PI model has also been extended to account for additional sources of environmental heterogeneity due to vascular remodeling, and, as with the Greenspan model, spatial variation in local oxygen levels. The resulting proliferation–invasion–hypoxia–necrosis–angiogenesis (PIHNA) model extends (28) by including additional PDEs to describe the distributions of hypoxic glioma cells, necrotic matter, blood vessel density, and angiogenic factors [46]. As with the modified Greenspan model, changes in the cell kill rate due to radiotherapy as oxygen levels vary can be incorporated via the modified LQ model defined by (25) and (26) (see [48]).

C. Model Extensions

As with the ODE models, the PDE models described above can be extended in multiple ways. Additional equations can be included to account for additional species

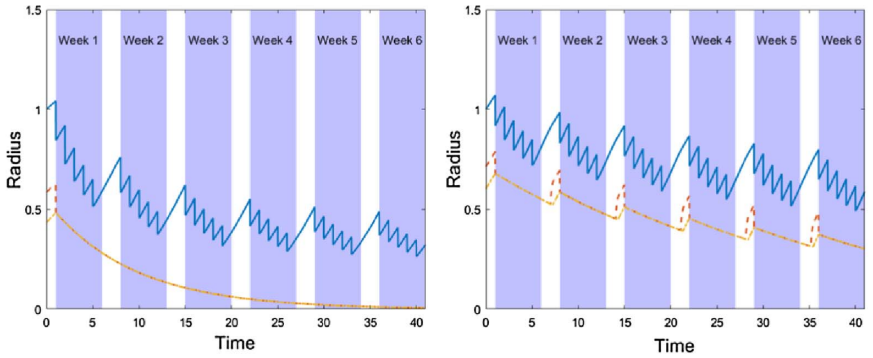

Fig. 5. *Numerical solutions of the Greenspan model, showing how the response to a standard, six-week, fractionation protocol (2-Gy fractions delivered daily Monday–Friday, shown as shaded regions) changes when the rate of natural, or apoptotic, cell death (μ_A) declines; at the end of treatment, the tumor with the smaller rate of natural cell death (right-hand size) is larger and retains a necrotic core, whereas the tumor with the larger rate of natural cell death (left-hand side) is smaller and the size of its necrotic core is negligible. Key: the outer tumor radius; R(t): blue solid line and the hypoxic radius, and $R_H(t)$: red dashed line; the necrotic core radius; $R_N(t)$: yellow dot/dashed line. Reproduced from [44, Fig. 4].*

(e.g., immune cells and blood vessels) and treatment combinations (e.g., radiotherapy, virotherapy, chemotherapy, and/or immunotherapy [49]).

With increasing evidence that tumor cells are sensitive to mechanical stimuli, other authors have developed biomechanical models in which the tumor is viewed as a mixture of interacting phases. Mass and momentum balances are applied to each phase, and appropriate constitutive laws are used to describe their mechanical properties. Multiphase models have been used to study vascular tumor growth [50] and the response of avascular tumors to radiotherapy and virotherapy [51], [52]. They have also been used to show how growth-induced compression of a compliant tissue matrix that surrounds a tumor spheroid can generate restraining forces that inhibit its growth, even when nutrients are freely available [53]. In future work, they could be used to study the efficacy of therapies designed to alter the mechanical properties of the tissue surrounding a tumor by, for example, neutralizing the action of matrix-degrading proteases that facilitate continued tumor growth and invasion [9]. With their origins in physics, phase-field models represent an exciting alternative to multiphase models [54], [55]. A key advantage of phase-field models is their ability to accommodate topological changes caused by, for example, the disappearance of a tumor following successful radiotherapy, or the emergence of new blood vessels during angiogenesis.

V. AGENT-BASED MODELS

While PDE models can describe spatial heterogeneity, they are unable to account for some important aspects of tumor biology. In particular, they cannot resolve individual cells and, therefore, cannot explore situations for

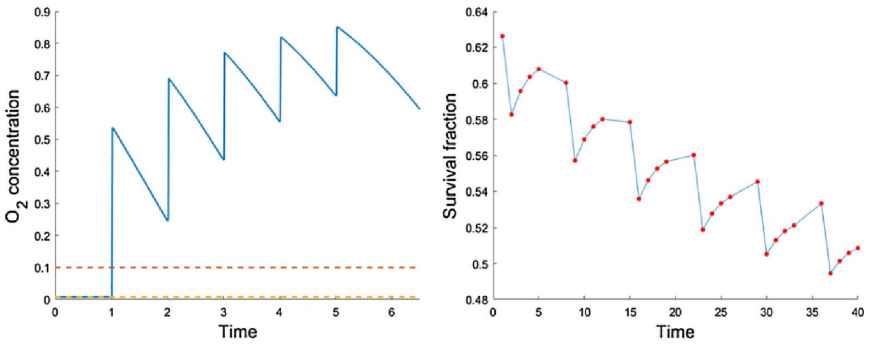

Fig. 6. *Additional results associated with the simulation from the right-hand side of Fig. 5. Left-hand side: this plot shows how, during the early stages of treatment, the oxygen concentration within the necrotic core fluctuates, and how, as the tumor shrinks in size, the average oxygen concentration rises above the necrotic and hypoxic thresholds, c_H (dashed orange line) and c_N (dashed yellow line). Right-hand side: this plot shows how the volume-averaged tumor survival fraction changes during the six-week fractionation protocol. Key: red points correspond to the survival fraction when each radiotherapy dose is delivered, the blue line added for ease of visualization. Reproduced from [44, Fig. 5].*

which cell level differences are important. Tumors are multiscale, and their growth dynamics and response to treatment are influenced by crosstalk between tissue-scale processes (e.g., angiogenesis, vascular remodeling, and blood flow) and subcellular ones (e.g., cytokine production and the effect of local nutrient levels on cell cycle progression). In order to account for subcellular effects, discrete models that resolve individual cells have been developed. These models are often termed agent-based models (ABMs). They admit cell–scale spatial resolution and can accommodate detailed subcellular, cell–cell, and cell–microenvironmental processes. Many ABMs combine continuum and discrete approaches to account for processes at different biological scales (and their interactions). Such *hybrid* models of tumor growth and radiotherapy typically treat cells as discrete entities and associate with them subcellular models that govern cell behavior in response to microenvironmental cues and radiotherapy. The subcellular models may be stochastic, or they may comprise deterministic ODEs. PDEs are commonly used to describe the distribution of nutrients, such as oxygen and glucose (and chemotherapeutic drugs) at the tissue scale, with the discrete cells acting as point sources or sinks. The spatial distributions of the diffusible species may, in turn, influence the behavior of individual cells at the subcellular level. While hybrid models can be biologically detailed, their complexity comes with an increasing computational cost and larger numbers of parameters, which can make them challenging to simulate, validate, and fit to data.

The behavior of the agents depends on the modeling framework. Several important choices must be made: whether to use an on-lattice framework (in which agents are confined to locations on a regular grid) or an off-lattice framework (in which agents move freely in space); whether to represent cells by the positions of their cell centers or to explicitly account for their shape. Common choices of lattice-based models include cellular automata and cellular Potts models [56], while off-lattice models include Voronoi methods, overlapping-spheres models, and vertex-based models [57].

While some ABMs are developed from scratch, it is increasingly common to use pre-existing software to construct ABMs. Exploiting existing software is particularly important when complex models are required, as errors in the underlying model implementation are less likely to be introduced and more likely to be identified in large, open-source software collaborations. Available software packages include Cancer, Heart and Soft Tissue Environment (Chaste) [58], which implements a range of different ABMs; Physicell [59], which combines an overlapping spheres model for individual cells with BioFVM [60] to accommodate interactions between cells and multiple diffusible species, such as oxygen; and Hybrid Automata Library (HAL) [61], a JAVA-based library with modular hybrid modeling capabilities and efficient visualization tools. Other tools include Morpheus [62] and Biocellion [63].

In Fig. 7, we present a schematic of an off-lattice ABM to show how such models are composed and how tissue, cell, and subcellular processes may interact. The model describes macrophage infiltration into a tumor spheroid in response to spatial gradients of colony-stimulating factor-1 (CSF-1), a chemoattractant produced by hypoxic tumor cells. At the tissue level, PDEs describe the diffusive transport, production, and consumption of oxygen and CSF-1, with tumor cells acting as point sinks of oxygen and point sources of CSF-1 if their local oxygen levels are low. The distributions of oxygen and CSF-1 modulate the cell and subcellular behaviors of the individual cells. For example, macrophages experience a "chemotactic force" in the direction of increasing CSF-1 gradients. In addition, the local oxygen concentration influences the tumor cells' phenotypes and, thereby, their progress through the cell cycle. Subcellular processes also influence cell-level processes, with new cells being produced at the end of the cell cycle, and interaction forces between neighboring cells depending on their phenotypes.

In the remainder of this section, we present examples of both on- and off-lattice ABMs and show how their increased spatial resolution allows more detailed descriptions of radiotherapy than is feasible with ODE and PDE models.

A. On-Lattice Models

On-lattice models restrict the location of agents to a discrete set of lattice points. These points are typically a square lattice although triangular or hexagonal meshes are sometimes used. On-lattice ABMs have several advantages: they are relatively simple to implement and, therefore, computationally efficient to simulate. They leverage the power of an ABM to incorporate cell–scale spatial heterogeneity and subcellular phenomena without requiring detailed consideration of the biomechanical forces that act on individual cells.

Cellular automaton (CA) models are arguably the most common and simplest type of on-lattice models. They typically assume that each cell occupies a single lattice site. The occupancy of the lattice sites is updated at discrete timesteps, which may range from seconds to hours, depending on the biological processes of interest. For example, on a given timestep, a tumor cell may attempt to proliferate with probability p_1 by placing a daughter cell into an adjacent empty lattice site, it may attempt to move to an adjacent empty site with probability p_2, and it may do nothing with probability $1 - p_1 - p_2$. The probabilities p_1 and p_2 may be fixed or may depend on the subcellular status of an individual cell (e.g., proliferation may occur only if a cell has completed its cell cycle) and its local microenvironment (e.g., a cell's movement may be biased up spatial gradients of a chemoattractant). While many on-lattice models can be described as cellular automata, we note that cellular Potts models, in which each biological cell occupies multiple neighboring lattice sites, represent

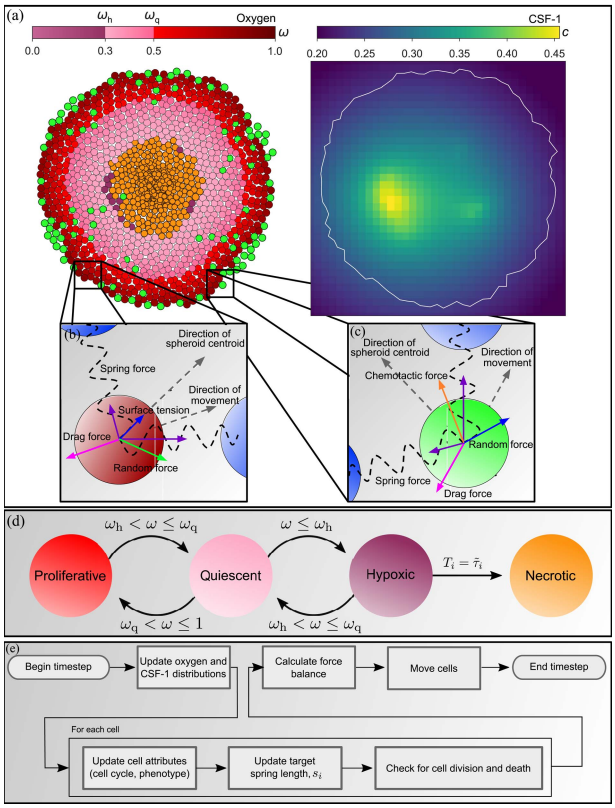

Fig. 7. ***Schematic showing how tissue-level, cell-level, and subcellular components may interact within an ABM. In this model, individual cells form (a) tumor spheroid and consume oxygen as it diffuses from the spheroid boundary. The distributions of oxygen and the macrophage chemoattractant CSF-1 (produced by hypoxic tumor cells) are calculated at the tissue level. (b) Tumor cells and (c) macrophages exert mechanical forces on each other. Additional forces act on the agents and may depend on the tissue-level chemical distributions: for example, the chemotactic force experienced by each macrophage depends on the local gradient of CSF-1. The net force on a cell determines its movement at each timestep. (d) How local oxygen levels influence tumor cell phenotype at the subcellular scale. The flowchart in (e) summarizes how the ABM is updated on each timestep. Reproduced from [64, Fig. S1].***

an alternative on-lattice framework that has also been used to simulate the effects of radiation therapy on tumors (see [65]).

In the context of radiotherapy, on-lattice models that include subcellular cell-cycle models can include more detailed descriptions of cell kill in response to treatment. For example, Brüningk *et al.* [66] use a CA framework to simulate therapies that combine radiation with hyperthermia. The virtual cells in their model have an internal cell cycle consisting of G1, S, G2, and M-phases, and the progress through the phases is based on an internal timer. Cells enter a quiescent G0 phase, during which their cell cycle is paused, if there are no free spaces in their neighborhood, and resume cycling when free spaces become available. The LQ model used in continuum models to determine the fraction of cells that survive exposure to radiotherapy is replaced by a stochastic model, which defines the probability that an individual cell survives exposure to a dose d of radiotherapy. This model accounts for both local oxygen levels c and cell cycle phase, represented by γ [66], and takes the form

$$\mathrm{SF}(c) = \exp\left(-\gamma \cdot \left(\alpha \cdot \frac{d}{\mathrm{OER}(c)} + \beta \cdot \frac{d^2}{\mathrm{OER}^2(c)}\right)\right) \tag{30}$$

where

$$\mathrm{OER}(c) = \begin{cases} 1, & \text{if } c > 11 \text{ mmHg} \\ 3 - \dfrac{2 \cdot c}{11}, & \text{if } c \leq 11 \text{ mmHg}. \end{cases} \tag{31}$$

An advantage of this model compared to the LQ model is that, following radiation damage, cell death is not necessarily instantaneous. Rather, when a dose of radiotherapy is given, each agent samples a random number N that lies between 0 and 1. If $N > \mathrm{SF}(c)$, the cell is labeled for death but only dies when the cell attempts to divide at the end of the cell cycle. If, during this time, the cell becomes quiescent due to a lack of oxygen, it remains alive until its cell cycle reaches the M-phase, and then, cell death is induced.

B. Off-Lattice Models

While cellular automata models provide a relatively computationally efficient means of introducing subcellular effects and stochasticity into models of cancer, they cannot describe complex spatial interactions between neighboring cells or accurately account for the forces between them. These forces arise through mechanisms, such as intercellular adhesion or volume exclusion. On-lattice models are generally unsuitable for exploring these types of interactions, and so off-lattice models in which agents move around a domain without restriction to a lattice are used when these forces may be important. For instance, in the example shown in Fig. 7, an off-lattice model was used in order to account for tumour cells obstructing macrophage chemotaxis and also advective movement caused by tumor cell proliferation and death of tumor cells. Off-lattice models are generally more computationally intensive than on-lattice ones but are able to capture a more realistic range of interactions between individual cells.

For example, Kempf *et al.* [67] use a 3-D off-lattice model of tumor spheroid growth to understand how radiation may drive cell cycle synchronization and how this could be exploited by subsequent radiation treatments to increase cell kill. They use a Voronoi–Delaunay approach in which the shapes of individual cells can be defined from the positions of their centers. A subcellular model governs progress through the cell cycle and includes two checkpoints at which the cell cycle can be paused. During the G2/M-phase, cells that have been damaged by radiation die, either immediately or via apoptosis at the G2 checkpoint. The second checkpoint is during the G1

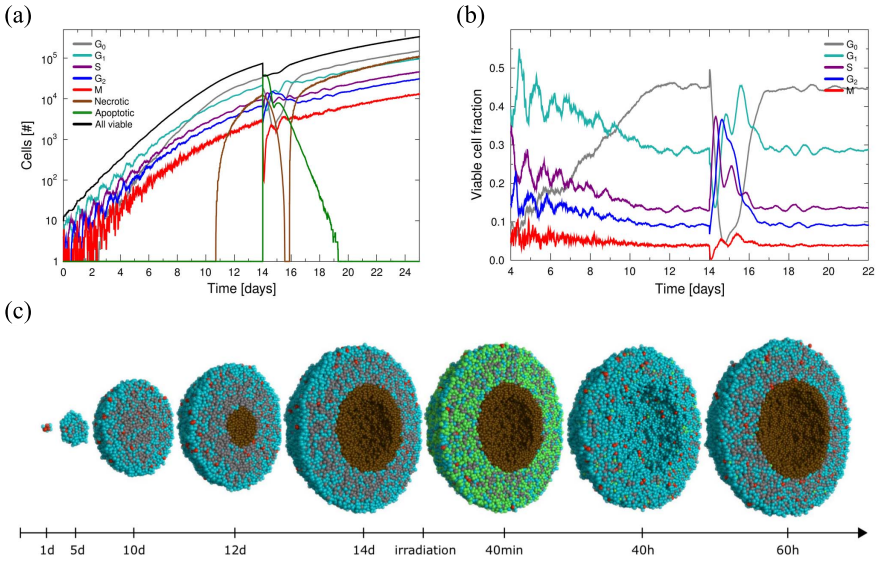

Fig. 8. *Response of a spheroid to 4 Gy of radiation. (a) and (b) Effects of radiation on redistribution of cell cycles, one of the five R's of radiotherapy. (c) Cross-section through the spheroid. A small number of cells rapidly grow into a solid tumor spheroid, with quiescent cells in high-density regions. Once the spheroid is large enough, nutrient deprivation causes cells in the center to die and form a necrotic core. After irradiation, many cells become apoptotic, leading to a gradual reduction in spheroid size and sufficient reoxygenation to reactive quiescent cells. Finally, the cell density increases until the necrotic core reestablishes itself. Key: cyan = G1, S, or G2-phase; red = mitotic cells; gray = quiescent cells; brown = necrotic cells; and green = apoptotic cells. Figure reproduced from [68, Fig. 2].*

phase, during which cells become quiescent if their internal pressure is sufficiently high. This mechanism mimics contact inhibition of growth when cells experience high intercellular forces from their neighbors. As with the models described above, this model also accounts for cell death and quiescence due to insufficient tissue-level concentrations of oxygen and glucose, with their distributions being described via PDEs. A typical model simulation, showing how a tumor responds to irradiation, is presented in Fig. 8. In common with the ABM models described above, Kempf *et al.* [67] use a variant of the LQ model to determine the cell survival fraction: they assume that the survival fraction depends on the cell cycle phase so that

$$\mathrm{SF}_p = \exp\left(-\left(\alpha_p d + \beta_p d^2\right)\right) \tag{32}$$

where p indicates the cell cycle phase (G1, S, G2, or M), and α_p and β_p are cell cycle phase-specific constants.

C. Model Extensions

The on- and off-lattice models described above show how ABMs can be used to add subcellular complexity to models of cancer growth and treatment. Due to their multiscale nature, these models can be extended to account for additional subcellular and tissue-scale behaviors as embodied in the Hallmarks of Cancer (see Fig. 1). In this section, we outline some extensions to ABMs that highlight this ability.

One of the Hallmarks of Cancer is "genomic instability and mutation." Mutational status can be represented as a subcellular property of an ABM. For example, coupling the subcellular process with ABMs is necessary to account for the emergence of resistance in cell populations. Resistance to therapy is gained via random mutations that confer an advantage to the resulting cell population. Since these mutations are stochastic, the proportion of cells in a tumor that is resistant to treatment may initially be too small to accurately describe using continuum approaches. Similarly, if a mutation that confers radioresistance also reduces a cell's proliferation rate, then the mutant cell population may die out before treatment is applied. In this way, the stochasticity of an ABM may help explain why radiotherapy successfully eliminates some patients' tumors, while, in other patients, small populations of radio-resistant cells drive relapse following treatment.

The second hallmark of cancer, "inducing angiogenesis," suggests a way in which the ABMs described here could be extended at the tissue scale by including vasculature. For example, Grogan *et al.* [69] consider the impact of vascular geometry on cell growth and response to radiotherapy. Fig. 9 shows three representations of a vascular network. The different geometries are used to simulate the oxygen distribution within the tissue and the impact of radiotherapy on the constituent tumor cells. ABMs can also be coupled to detailed models of tumor blood flow, angiogenesis, and vascular remodeling to understand their impact on tumor heterogeneity and the emergence of hypoxic regions [70]. Such detailed ABMs also permit investigation of treatments in which radiotherapy is combined with other treatments, including hypoxia-activated prodrugs [71].

VI. INTEGRATING MATHEMATICAL MODELS WITH DATA

In Sections III–V, we introduced ODE, PDE, and ABM models of solid tumor growth and focused on the qualitative insight that they can generate. In order to realize their full potential, the models should be validated against appropriate data (see Fig. 3). Until recently, this has proven a significant challenge to the integration of mathematical models with clinical decision-making and/or experimental research. As we explain below, there are encouraging signs that the landscape is changing.

Although advances in medical imaging enable the collection of more detailed data, most patient data are relatively low resolution. For example, routine CT scans provide approximate measurements of tumor volume, with high levels of uncertainty. Such data can be used to parameterize simple ODE models but are inadequate for accurate parameterization of spatial models. While higher resolution imaging techniques will aid the parameterization of more complex models, parameter estimation remains a major bottleneck to the wider integration of mathematical models into clinical practice. As such, more complex models are often calibrated against experimental data to estimate parameter values that subsequently inform clinical models [72]. Automated image analysis tools can also be integrated into the mathematical modeling process to enable more accurate data fitting and model selection [73].

Integrating models with clinical data can provide new insight in situations where treatment yields unexpected behaviors. For example, the patient data presented in Fig. 10 does not conform to the 'sawtooth' dynamics that single-compartment ODE models produce (see Fig. 4).

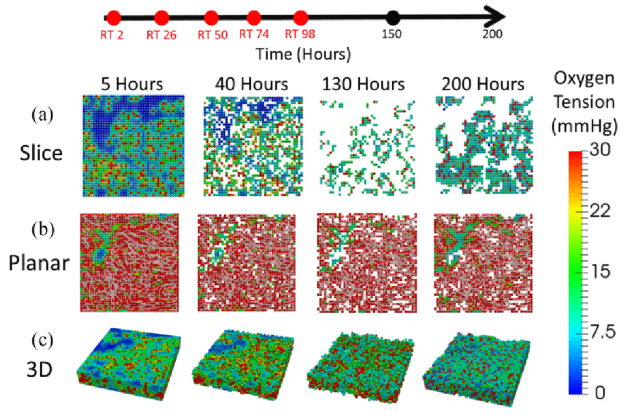

Fig. 9. *Influence of geometry on cell growth and response to RT. Simulations at times $t = 5$, 40, 130, and 200 h, comparing the response of tumor cells embedded in (a) "slice," (b) "planar," and (c) "3-D" representations of one of the biological networks to five rounds of daily RT. Administration times are also indicated. Cellular oxygen tension in mmHg is contoured. Parameter values: as per [69, Table 1], except for the oxygen consumption rate that is increased by a factor of 15 (from $k = 13\ \text{min}^{-1}$ to $k = 195\ \text{min}^{-1}$). Figure reproduced from [69, Fig. 4].*

In part, this difference is due to the time resolution of the clinical data. The data points in Fig. 10 are separated by at least one week, whereas the sawtooth dynamics occur on shorter timescales when radiotherapy is delivered daily. However, differences in temporal resolution cannot fully explain why the clinical data do not always conform to "sawtooth" dynamics. For instance, in some patients, the tumor volume initially increases during treatment and only starts to decrease midway through treatment. Such dynamic behavior cannot be captured by the sawtooth dynamics depicted in Figs. 4–6. By fitting the ODE model defined by (13) and (14) to this patient data, Lewin *et al.* [41] showed that such behavior may arise if dead cells are not removed instantaneously following radiotherapy. Fig. 10 also shows the value of using Bayesian methods to obtain *distributions* of parameter estimates rather than specific, pointwise values, as these posterior distributions can be used to identify 95% credible intervals around the model predictions.

Although parameter estimation remains challenging, fitting patient-specific parameters to mathematical models provides an opportunity to personalize treatment [74], [75]. Enderling and colleagues [32] are currently running a clinical trial (NCT03656133) in which the logistic growth model is fit to pretreatment data to estimate patient-specific parameter values that are used to assign patients to different radiotherapy protocols (e.g., hypofractionation and hyperfractionation, when the same total dose of radiation is given in a large number of small doses or a small number of large doses) [71]. Mathematical models can also be used to identify optimal treatment protocols that may differ from the standard of care. After fitting patient-specific parameters to a mathematical model, optimal control theory can be used to propose optimal treatments that, for example, maximize expected tumor volume reduction while minimizing the total radiation dose applied to the patient [76].

Mathematical models can also be used to conduct "virtual clinical trials" in which virtual patient cohorts, characterized by distributions of model parameter values, are exposed to different treatments parameters, and the expected range of treatment outcomes predicted, during trial design. Virtual trials can also be used to establish what data should be collected to reliably quantify patient responses to the different treatments. In this way, the targeted use of mathematical modeling has the potential to enable clinicians to identify and correct potential weaknesses in trial design.

As the use of medical resonance imaging (MRI) and positron emission tomography increases, access to spatially resolved data that can detect tumor boundaries and show how they change over time is becoming available to clinicians and mathematical modelers. As these data have limited spatial resolution and are unable to resolve individual cells, PDE models represent a natural framework for interpreting such images. For example, in Fig. 11, the proliferation-invasion model was used to simulate glioma

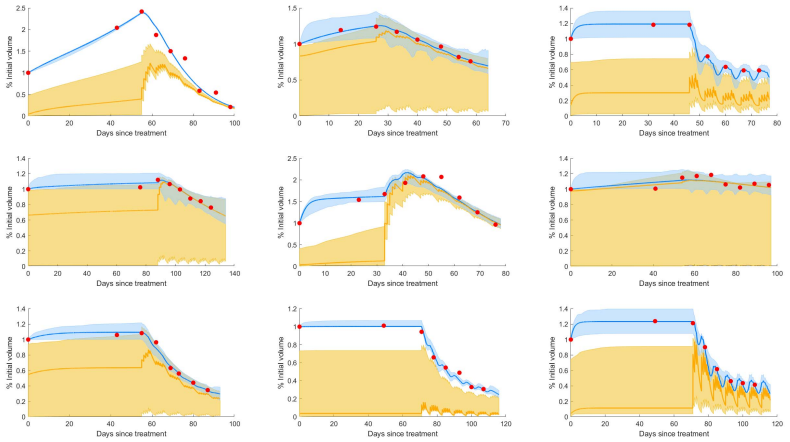

Fig. 10. *Results obtained by fitting the two-compartment model defined by (13) and (14) to clinical patient data using the approximate Bayesian computation sequential Monte Carlo (ABC SMC) algorithm. The blue and yellow curves show the total tumor and necrotic volume for simulations using the best-fitting parameter sets. At each time point, the 95% credible intervals for the total tumor and necrotic volume (blue and yellow regions, respectively) are obtained by sampling 120 parameter combinations from the posterior distributions. Clinical data points are marked by red filled circles. Figure reproduced from [41, Fig. 3].*

growth and model outputs compared to MRI images [77]. The mathematical model is termed an untreated virtual control (UVC). The UVC uses pretreatment scans to simulate how tumor development may have continued in the absence of treatment, allowing clinicians to assess how well treatment is working based on deviations between posttreatment measurement and the UVC. This example highlights a further benefit of using mathematical modeling in the clinic: since medical images have limited spatial resolution, they can only detect tumor regions where the density exceeds a threshold value. By contrast, mathematical models can "see" below such threshold values and more accurately predict the true extent of tumor invasion and spread.

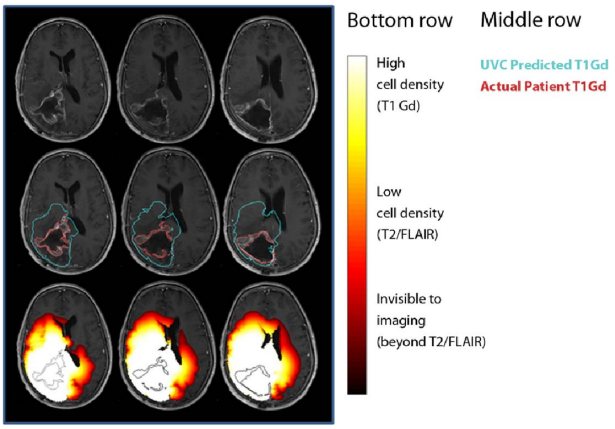

Fig. 11. *Comparisons between UVCs and posttreatment MRI scans. First row: posttreatment MRI. Second row: contours showing measured tumor on T1-Gd-enhanced scan (red) and UVC prediction of T1-Gd area (aqua). Third row: UVC tumor cell densities overlaid (white: high cell density and red: low cell density) on scan with T1-Gd measured tumor outline (black). Figure reproduced from [77, Fig. 7].*

Outside the clinic, techniques such as imaging mass cytometry and multiplex immunohistochemistry can generate spatial images that resolve the expression of specific proteins at cellular and subcellular resolutions. By integrating such images with single-cell RNA sequencing data, it is now possible to collect exquisitely detailed experimental data at subcellular, cellular, and tissue scales. Such data are ideally suited for parameterizing and validating multiscale models that can be used to help develop new therapies and drive fundamental research into our understanding of tumor growth and development.

VII. CONCLUSION

In this article, we have reviewed a range of mathematical models that describe tumor growth and response to radiotherapy and illustrated the mechanistic insight that they can generate. In the same way that Hanahan and Weinberg's Hallmarks of Cancer provide a guiding principle for characterizing different cancers, we now propose six Hallmarks of Mathematical Oncology that can be used to characterize mathematical models: discrete or continuous variables, deterministic or stochastic, single- or multiscale, spatially averaged or spatially resolved, homogeneous or heterogeneous, and single or hybrid framework (see Fig. 2).

Confronted by the array of mathematical approaches being used to study tumor growth, it can be difficult to know what approach and level of detail to use. The situation can be compounded when different models are equally compatible with the experimental data. In practice, such decisions depend on the questions under investigation and the available data. In general, cell-based models can be more easily extended to account for additional data

on subcellular signaling pathways and/or the cell cycle, whereas coarser-grained PDE and spatially averaged ODE models contain fewer parameters and, as a result, should yield more robust fits to the data. While complex models, with multiple parameters, may overfit experimental data, they can act as surrogates for experimental data with the advantage that there is a known "ground truth" against which to test the predictive accuracy of simpler models. Care must, therefore, be taken to balance model complexity against the availability of experimental data. In addition, if model simulations from different approaches yield qualitatively different behavior (such as their predicted response of a multicellular spheroid to exposure to a particular drug), then these can be used to design experiments that discriminate between the alternative models.

In practice, close collaboration between theoreticians and biomedical researchers is crucial throughout this process because the models are only ever as good as the assumptions used to construct them and the data with which they are validated. Indeed, in many respects, the form of the initial model is less important than starting the dialog between experimentalists and modelers because any model is almost certain to be wrong!

In conclusion, mathematical models represent a natural framework for not only testing biological hypotheses and generating new ones but also optimizing experimental protocols. As we survey the large body of research devoted to modeling tumor growth, it is clear that considerable progress has been made. Many mathematical and computational tools (or models) have been developed: what is now needed is to translate these prototypes into validated models that are specialized for particular tumors and treatments, and have the power to generate qualitative and quantitative predictions. The increasing number of modeling papers appearing in the literature indicates that this transition is starting to happen. ■

REFERENCES

[1] H. Sung *et al.*, "Global cancer statistics 2020: GLOBOCAN estimates of incidence and mortality worldwide for 36 cancers in 185 countries," *CA, A Cancer J. Clinicians*, vol. 71, no. 3, pp. 209–249, May 2021, doi: 10.3322/caac.21660.

[2] D. Hanahan and R. A. Weinberg, "The hallmarks of cancer," *Cell*, vol. 100, no. 1, pp. 57–70, 2000. [Online]. Available: http://www.ncbi.nlm.nih.gov/pubmed/10647931

[3] D. Hanahan and R. A. Weinberg, "Hallmarks of cancer: The next generation," *Cell*, vol. 144, no. 5, pp. 646–674, 2011. [Online]. Available: http://www.ncbi.nlm.nih.gov/pubmed/21376230

[4] H. Enderling, J. C. L. Alfonso, E. Moros, J. J. Caudell, and L. B. Harrison, "Integrating mathematical modeling into the roadmap for personalized adaptive radiation therapy," *Trends Cancer*, vol. 5, no. 8, pp. 467–474, Aug. 2019, doi: 10.1016/j.trecan.2019.06.006.

[5] L. Preziosi, *Cancer Modelling and Simulation*. London, U.K.: Chapman & Hall, 2003.

[6] D. Wodarz and N. L. Komarova, *Computational Biology of Cancer*. Singapore: World Scientific, 2005.

[7] J. Folkman and M. Hochberg, "Self-regulation of growth in three dimensions," *J. Experim. Med.*, vol. 138, no. 4, pp. 745–753, Oct. 1973, doi: 10.1084/jem.138.4.745.

[8] M. De Palma, D. Biziato, and T. V. Petrova, "Microenvironmental regulation of tumour angiogenesis," *Nature Rev. Cancer*, vol. 17, no. 8, pp. 457–474, Aug. 2017, doi: 10.1038/nrc.2017.51.

[9] W. G. Stetler-Stevenson, "The tumor microenvironment: Regulation by MMP-independent effects of tissue inhibitor of metalloproteinases-2," *Cancer Metastasis Rev.*, vol. 27, no. 1, pp. 57–66, Mar. 2008, doi: 10.1007/s10555-007-9105-8.

[10] F. Perri, S. Pisconti, and G. D. V. Scarpati, "P53 mutations and cancer: A tight linkage," *Ann. Transl. Med.*, vol. 4, no. 24, pp. 522–522, Dec. 2016, doi: 10.21037/atm.2016.12.40.

[11] I. Turesson *et al.*, "Biological response to radiation therapy," *Acta Oncolog.*, vol. 42, no. 2, pp. 92–106, Mar. 2003, doi: 10.1080/02841860310004959.

[12] R. G. Dale, "Dose-rate effects in targeted radiotherapy," *Phys. Med. Biol.*, vol. 41, no. 10, pp. 1871–1884, Oct. 1996, doi: 10.1088/0031-9155/41/10/001.

[13] M. G. Haddock, "Intraoperative radiation therapy for colon and rectal cancers: A clinical review," *Radiat. Oncol.*, vol. 12, no. 1, pp. 1–8, Dec. 2017, doi: 10.1186/s13014-016-0752-1.

[14] G. G. Steel, "The search for therapeutic gain in the combination of radiotherapy and chemotherapy," *Radiotherapy Oncol.*, vol. 11, pp. 31–53, Jan. 1988, doi: 10.1016/0167-8140(88)90044-8.

[15] S. C. Brüningk, I. Rivens, C. Box, U. Oelfke, and G. ter Haar, "3D tumour spheroids for the prediction of the effects of radiation and hyperthermia treatments," *Sci. Rep.*, vol. 10, no. 1, pp. 1–13, Dec. 2020, doi: 10.1038/s41598-020-58569-4.

[16] M. Muthana *et al.*, "Macrophage delivery of an oncolytic virus abolishes tumor regrowth and metastasis after chemotherapy or irradiation," *Cancer Res.*, vol. 73, no. 2, pp. 490–495, Jan. 2013, doi: 10.1158/0008-5472.CAN-12-3056.

[17] E. J. Van Limbergen *et al.*, "Combining radiotherapy with immunotherapy: The past, the present and the future," *Brit. J. Radiol.*, vol. 90, no. 1076, Aug. 2017, Art. no. 20170157, doi: 10.1259/bjr.20170157.

[18] P. Hoskin, M. Saunders, and S. Dische, "Hypoxic radiosensitizers in radical radiotherapy for patients with bladder carcinoma," *Cancer*, vol. 86, pp. 1322–1328, Oct. 1999, doi: 10.1002/(SICI)1097-0142(19991001)86:7.1322:AID-CNCR30.3.0.CO.2-E.

[19] M. Skwarski, E. Bowler, J. D. Wilson, G. S. Higgins, and E. M. Hammond, *Targeting Tumor Hypoxia*. Cham, Switzerland: Springer, 2020, pp. 265–299, doi: 10.1007/978-3-030-49701-9.11.

[20] D. J. Brenner, "The linear-quadratic model is an appropriate methodology for determining isoeffective doses at large doses per fraction," *Seminars Radiat. Oncol.*, vol. 18, no. 4, pp. 234–239, Oct. 2008, doi: 10.1016/j.semradonc.2008.04.004.

[21] D. J. Brenner, L. R. Hlatky, P. J. Hahnfeldt, Y. Huang, and R. K. Sachs, "The linear-quadratic model and most other common radiobiological models result in similar predictions of time-dose relationships," *Radiat. Res.*, vol. 150, no. 1, pp. 83–91, 1998, doi: 10.2307/3579648.

[22] G. G. Steel, T. J. Mcmillan, and J. H. Peacock, "The 5Rs of radiobiology," *Int. J. Radiat. Biol.*, vol. 56, no. 6, pp. 1045–1048, Jan. 1989, doi: 10.1080/09553008914552491.

[23] E. Hall and A. Giaccia, *Radiobiology for the Radiobiologist*, 7th ed. Philadelphia, PA, USA: Lippincott, Williams and Wilkins, 2011.

[24] M. Joiner and A. van der Kogel, *Basic Clinical Radiobiology*, 4th ed. London, U.K.: Hodder Arnold, 2009.

[25] A. V. Ponce Bobadilla, P. K. Maini, and H. Byrne, "A stochastic model for tumour control probability that accounts for repair from sublethal damage," *Math. Med. Biol., J. IMA*, vol. 35, no. 2, pp. 181–202, Jun. 2018, doi: 10.1093/imammb/dqw024.

[26] R. G. Dale, "A new incomplete-repair model based on a 'reciprocal-time' pattern of sublethal damage repair," *Acta Oncolog.*, vol. 38, no. 7, pp. 919–929, Jan. 1999, doi: 10.1080/028418699432608.

[27] A. Bertuzzi, A. Fasano, A. Gandolfi, and C. Sinisgalli, "Reoxygenation and split-dose response to radiation in a tumour model with Krogh-type vascular geometry," *Bull. Math. Biol.*, vol. 70, no. 4, pp. 992–1012, May 2008, doi: 10.1007/s11538-007-9287-9.

[28] H. Enderling and M. Chaplain, "Mathematical modeling of tumor growth and treatment," *Current Pharmaceutical Des.*, vol. 20, pp. 40–4934, Sep. 2014, doi: 10.2174/1381612819666131125150434.

[29] J. Liu *et al.*, "A time-resolved experimental—Mathematical model for predicting the response of glioma cells to single-dose radiation therapy," *Integrative Biol.*, vol. 13, pp. 167–183, Jun. 2021, doi: 10.1093/intbio/zyab010.

[30] P. Castorina, T. S. Deisboeck, P. Gabriele, and C. Guiot, "Growth laws in cancer: Implications for radiotherapy," *Radiat. Res.*, vol. 168, no. 3, pp. 349–356, Sep. 2007, doi: 10.1667/RR0787.1.

[31] M. U. Zahid *et al.*, "Forecasting individual patient response to radiation therapy in head and neck cancer with a dynamic carrying capacity model," *Int. J. Radiat. Oncol. Biol. Phys.*, vol. 111, no. 3, pp. 693–704, Nov. 2021, doi: 10.1016/j.ijrobp.2021.05.132.

[32] S. Prokopiou *et al.*, "A proliferation saturation index to predict radiation response and personalize radiotherapy fractionation," *Radiat. Oncol.*, vol. 10, no. 1, p. 159, Dec. 2015, doi: 10.1186/s13014-015-0465-x. [Online]. Available: http://www.ro-journal.com/content/10/1/159

[33] M. Paczkowski *et al.*, "Reciprocal interactions between tumour cell populations enhance growth and reduce radiation sensitivity in prostate cancer," *Commun. Biol.*, vol. 4, no. 1, pp. 1–13, Dec. 2021, doi: 10.1038/s42003-020-01529-5.

[34] P. Hahnfeldt, D. Panigrahy, J. Folkman, and L. Hlatky, "Tumor development under angiogenic signaling," *Cancer Res.*, vol. 59, no. 19, pp. 4770–4775, 1999.

[35] R. K. Sachs, L. R. Hlatky, and P. Hahnfeldt, "Simple ODE models of tumor growth and anti-angiogenic or radiation treatment," *Math. Comput. Model.*, vol. 33, pp. 1297–1305, Jun. 2001, doi: 10.1016/S0895-7177(00)00316-2.

[36] V. A. Kuznetsov, I. A. Makalkin, M. A. Taylor, and A. S. Perelson, "Nonlinear dynamics of immunogenic tumors: Parameter estimation and

global bifurcation analysis," *Bull. Math. Biol.*, vol. 56, no. 2, pp. 295–321, Mar. 1994, doi: 10.1007/BF02460644.

[37] I. Butuc, C. Mirestean, and D. Iancu, "A nonlinear model in the dynamics of tumour-immune system combined with radiotherapy," *U.P.B. Sci. Bull., Ser. A*, vol. 81, pp. 311–322, Apr. 2019.

[38] A. Ghaffari, B. Bahmaie, and M. Nazari, "A mixed radiotherapy and chemotherapy model for treatment of cancer with metastasis," *Math. Methods Appl. Sci.*, vol. 39, no. 15, pp. 4603–4617, Oct. 2016, doi: 10.1002/mma.3887.

[39] S. M. Al-Tuwairqi, N. O. Al-Johani, and E. A. Simbawa, "Modeling dynamics of cancer radiovirotherapy," *J. Theor. Biol.*, vol. 506, Dec. 2020, Art. no. 110405, doi: 10.1016/j.jtbi.2020.110405.

[40] A. V. Chvetsov, S. Yartsev, J. L. Schwartz, and N. Mayr, "Assessment of interpatient heterogeneity in tumor radiosensitivity for nonsmall cell lung cancer using tumor-volume variation data," *Med. Phys.*, vol. 41, May 2014, Art. no. 064101, doi: 10.1118/1.4875686.

[41] T. Lewin, P. Maini, E. Moros, J. Caudell, H. Enderling, and H. Byrne, "Using mathematical modelling to identify data requirements for increased prediction accuracy in radiotherapy," 2022, *arXiv:2201.02101*.

[42] H. P. Greenspan, "Models for the growth of a solid tumor by diffusion," *Stud. Appl. Math.*, vol. 51, no. 4, pp. 317–340, Dec. 1972, doi: 10.1002/sapm1972514317.

[43] K. R. Swanson, E. Alvord, and J. Murray, "A quantitative model for differential motility of gliomas in grey and white matter," *Cell Proliferation*, vol. 33, no. 5, pp. 317–329, Oct. 2000. [Online]. Available: http://www.ncbi.nlm.nih.gov/pubmed/11063134

[44] T. D. Lewin, P. K. Maini, E. G. Moros, H. Enderling, and H. M. Byrne, "The evolution of tumour composition during fractionated radiotherapy: Implications for outcome," *Bull. Math. Biol.*, vol. 80, no. 5, pp. 1207–1235, May 2018, doi: 10.1007/s11538-018-0391-9.

[45] K. R. Swanson, E. C. Alvord, and J. D. Murray, "Virtual brain tumours (gliomas) enhance the reality of medical imaging and highlight inadequacies of current therapy," *Brit. J. Cancer*, vol. 86, no. 1, pp. 14–18, Jan. 2002, doi: 10.1038/sj.bjc.6600021. [Online]. Available: http://www.ncbi.nlm.nih.gov/pubmed/11857005

[46] K. R. Swanson, R. C. Rockne, J. Claridge, M. A. Chaplain, E. C. Alvord, and A. R. A. Anderson, "Quantifying the role of angiogenesis in malignant progression of gliomas: *In Silico* modeling integrates imaging and histology," *Cancer Res.*, vol. 71, no. 24, pp. 7366–7375, Dec. 2011, doi: 10.1158/0008-5472.CAN-11-1399.

[47] R. Rockne *et al.*, "Predicting the efficacy of radiotherapy in individual glioblastoma patients*in vivo*: A mathematical modeling approach," *Phys. Med. Biol.*, vol. 55, no. 12, pp. 3271–3285, Jun. 2010, doi: 10.1088/0031-9155/55/12/001.

[48] A. Hawkins-Daarud *et al.*, "*In silico* analysis suggests differential response to bevacizumab and radiation combination therapy in newly diagnosed glioblastoma," *J. Roy. Soc. Interface*, vol. 12, no. 109, 2015, Art. no. 20150388, doi: 10.1098/rsif.2015.0388.

[49] K. M. Storey, S. E. Lawler, and T. L. Jackson, "Modeling oncolytic viral therapy, immune checkpoint inhibition, and the complex dynamics of innate and adaptive immunity in glioblastoma treatment," *Frontiers Physiol.*, vol. 11, pp. 1–18, Mar. 2020, doi: 10.3389/fphys.2020.00151.

[50] M. E. Hubbard and H. M. Byrne, "Multiphase modelling of vascular tumour growth in two spatial dimensions," *J. Theor. Biol.*, vol. 316, pp. 70–89, Jan. 2013, doi: 10.1016/j.jtbi.2012.09.031.

[51] T. D. Lewin, H. M. Byrne, P. K. Maini, J. J. Caudell, E. G. Moros, and H. Enderling, "The importance of dead material within a tumour on the dynamics in response to radiotherapy," *Phys. Med. Biol.*, vol. 65, no. 1, Jan. 2020, Art. no. 015007, doi: 10.1088/1361-6560/ab4c27.

[52] M. A. Boemo and H. M. Byrne, "Mathematical modelling of a hypoxia-regulated oncolytic virus delivered by tumour-associated macrophages," *J. Theor. Biol.*, vol. 461, pp. 102–116, Jan. 2019, doi: 10.1016/j.jtbi.2018.10.044.

[53] C. Y. Chen, H. M. Byrne, and J. R. King, "The influence of growth-induced stress from the surrounding medium on the development of multicell spheroids," *J. Math. Biol.*, vol. 43, no. 3, pp. 191–220, Sep. 2001, doi: 10.1007/s002850100091.

[54] M. Fritz, E. A. B. F. Lima, V. Nikolić, J. T. Oden, and B. Wohlmuth, "Local and nonlocal phase-field models of tumor growth and invasion due to ECM degradation," *Math. Models Methods Appl. Sci.*, vol. 29, no. 13, pp. 2433–2468, Dec. 2019, doi: 10.1142/S0218202519500519.

[55] G. Vilanova, I. Colominas, and H. Gomez, "A mathematical model of tumour angiogenesis: Growth, regression and regrowth," *J. Roy. Soc. Interface*, vol. 14, no. 126, Jan. 2017, Art. no. 20160918, doi: 10.1098/rsif.2016.0918.

[56] F. Graner and J. A. Glazier, "Simulation of biological cell sorting using a two-dimensional extended Potts model," *Phys. Rev. Lett.*, vol. 69, pp. 2013–2017, 1992, doi: 10.1103/PhysRevLett.69.2013.

[57] J. M. Osborne, A. Fletcher, J. Pitt-Francis, P. Maini, and D. J. Gavaghan, "Comparing individual-based approaches to modelling the self-organization of multicellular tissues," *PLoS Comput. Biol.*, vol. 13, pp. 1–34, Feb. 2017, doi: 10.1371/journal.pcbi.1005387.

[58] F. Cooper *et al.*, "Chaste: Cancer, heart and soft tissue environment," *J. Open Source Softw.*, vol. 5, no. 47, p. 1848, Mar. 2020, doi: 10.21105/joss.01848.

[59] A. Ghaffarizadeh, R. Heiland, S. Friedman, and M. Shannon, "PhysiCell: An open source physics-based cell simulator for 3-D multicellular systems," *PLoS Comput. Biol.*, vol. 14, pp. 1–34, Feb. 2018, doi: 10.1371/journal.pcbi.1005991.

[60] A. Ghaffarizadeh, S. Friedman, and P. MacKlin, "BioFVM: An efficient, parallelized diffusive transport solver for 3-D biological simulations," *Bioinformatics*, vol. 32, no. 8, pp. 1256–1258, 2016, doi: 10.1093/bioinformatics/btv730.

[61] R. R. Bravo *et al.*, "Hybrid automata library: A flexible platform for hybrid modeling with real-time visualization," *PLOS Comput. Biol.*, vol. 16, no. 3, Mar. 2020, Art. no. e1007635, doi: 10.1371/journal.pcbi.1007635.

[62] J. Starruß, W. de Back, L. Brusch, and A. Deutsch, "Morpheus: A user-friendly modeling environment for multiscale and multicellular systems biology," *Bioinformatics*, vol. 30, no. 9, pp. 1331–1332, May 2014, doi: 10.1093/bioinformatics/btt772.

[63] S. Kang, S. Kahan, J. McDermott, N. Flann, and I. Shmulevich, "Biocellion: Accelerating computer simulation of multicellular biological system models," *Bioinformatics*, vol. 30, no. 21, pp. 3101–3108, Nov. 2014, doi: 10.1093/bioinformatics/btu498.

[64] O. Vipond *et al.*, "Multiparameter persistent homology landscapes identify immune cell spatial patterns in tumors," *Proc. Nat. Acad. Sci. USA*, vol. 118, no. 41, Oct. 2021, Art. no. e2102166118, doi: 10.1073/pnas.2102166118.

[65] X. Gao, J. T. McDonald, L. Hlatky, and H. Enderling, "Acute and fractionated irradiation differentially modulate glioma stem cell division kinetics," *Cancer Res.*, vol. 73, no. 5, pp. 1481–1490, Mar. 2013, doi: 10.1158/0008-5472.CAN-12-3429.

[66] S. C. Brüningk, P. Ziegenhein, I. Rivens, U. Oelfke, and G. T. Haar, "A cellular automaton model for spheroid response to radiation and hyperthermia treatments," *Sci. Rep.*, vol. 9, no. 1, pp. 1–12, Dec. 2019, doi: 10.1038/s41598-019-54117-x.

[67] H. Kempf, M. Bleicher, and M. Meyer-Hermann, "Spatio-temporal cell dynamics in tumour spheroid irradiation," *Eur. Phys. J. D*, vol. 60, no. 1, pp. 177–193, Oct. 2010, doi: 10.1140/epjd/e2010-00178-4.

[68] H. Kempf, H. Hatzikirou, M. Bleicher, and M. Meyer-Hermann, "*In silico* analysis of cell cycle synchronisation effects in radiotherapy of tumour spheroids," *PLoS Comput. Biol.*, vol. 9, no. 11, Nov. 2013, Art. no. e1003295, doi: 10.1371/journal.pcbi.1003295.

[69] J. A. Grogan *et al.*, "Predicting the influence of microvascular structure on tumor response to radiotherapy," *IEEE Trans. Biomed. Eng.*, vol. 64, no. 3, pp. 504–511, Mar. 2017, doi: 10.1109/TBME.2016.2606563.

[70] J. A. Grogan *et al.*, "Microvessel chaste: An open library for spatial modeling of vascularized tissues," *Biophys. J.*, vol. 112, no. 9, pp. 1767–1772, May 2017, doi: 10.1016/j.bpj.2017.03.036.

[71] S. Hamis, M. Kohandel, L. J. Dubois, A. Yaromina, P. Lambin, and G. G. Powathil, "Combining hypoxia-activated prodrugs and radiotherapy in silico: Impact of treatment scheduling and the intra-tumoural oxygen landscape," *PLOS Comput. Biol.*, vol. 16, no. 8, Aug. 2020, Art. no. e1008041, doi: 10.1371/journal.pcbi.1008041.

[72] E. A. B. F. Lima *et al.*, "Calibration of multi-parameter models of avascular tumor growth using time resolved microscopy data," *Sci. Rep.*, vol. 8, no. 1, Dec. 2018, Art. no. 14558, doi: 10.1038/s41598-018-32347-9.

[73] J. Yang *et al.*, "An experimental-mathematical approach to predict tumor cell growth as a function of glucose availability in breast cancer cell lines," *PLoS ONE*, vol. 16, no. 7, Jul. 2021, Art. no. e0240765, doi: 10.1371/journal.pone.0240765.

[74] J. B. West, M. N. Dinh, J. S. Brown, J. Zhang, A. R. Anderson, and R. A. Gatenby, "Multidrug cancer therapy in metastatic castrate-resistant prostate cancer: An evolution-based strategy," *Clin. Cancer Res.*, vol. 25, no. 14, pp. 4413–4421, Jul. 2019, doi: 10.1158/1078-0432.CCR-19-0006.

[75] J. Cunningham *et al.*, "Optimal control to reach eco-evolutionary stability in metastatic castrate-resistant prostate cancer," *PLoS ONE*, vol. 15, no. 12, Dec. 2020, Art. no. e0243386, doi: 10.1371/journal.pone.0243386.

[76] U. Ledzewicz, H. Maurer, and H. Schättler, "Optimal combined radio- and anti-angiogenic cancer therapy," *J. Optim. Theory Appl.*, vol. 180, no. 1, pp. 321–340, Jan. 2019, doi: 10.1007/s10957-018-1426-y.

[77] A. L. Baldock *et al.*, "From patient-specific mathematical neuro-oncology to precision medicine," *Frontiers Oncol.*, vol. 3, p. 62, Apr. 2013, doi: 10.3389/fonc.2013.00062.

ABOUT THE AUTHORS

Joshua Adam Bull received the B.A. degree in philosophy and mathematics from the University of Southampton, Southampton, U.K., in 2012, the M.Sc. degree in mathematical sciences from Durham University, Durham, U.K., in 2014, and the D.Phil. degree from the Systems Approaches to Biomedical Science Doctoral Training Centre, University of Oxford, Oxford, U.K., in 2018.

He is a Postdoctoral Researcher with the Mathematical Institute, University of Oxford, where his research focuses on developing novel mathematical and statistical approaches for image analysis and statistical description of multiplexed histological images. He also has strong interests in multiscale modeling and the integration of mathematical models with biomedical imaging data.

Helen Mary Byrne received the M.A. degree in mathematics from the University of Cambridge, Cambridge, U.K., in 1987, and the M.Sc. and D.Phil. degrees from the University of Oxford, Oxford, U.K., in 1988 and 1991, respectively.

After postdoctoral research at the University of Oxford and the University of Bath, Bath, U.K., she held lectureships at The University of Manchester Institute of Science and Technology (UMIST), Manchester, U.K., and the University of Nottingham, Nottingham, U.K., and was promoted to Professor in 2003. In Nottingham, she established and led the Centre for Mathematical Medicine and Biology before returning to the University of Oxford in 2011, where she is currently with the Mathematical Institute. Her research is focused on the development, analysis, and simulations of continuum and multiscale models of biomedical systems, with particular emphasis on the growth and response to treatment of solid tumors.

Dr. Byrne was made a Fellow of the Society for Mathematical Biology for her contributions to mathematical biology. She received the Leah Edelstein-Keshet Award. She was awarded an Advanced Research Fellowship from the United Kingdom's Engineering and Physical Sciences Research Council from 2000 to 2006.